SRTTU

JCARME
ISSN: 2228-7922

Journal of Computational and Applied Research
in Mechanical Engineering
Vol. 2, No. 1, pp. 37-49, Sept. 2012
http://jcarme.srttu.edu

Comparing thermal enhancement of Ag-water and SiO_2-water nanofluids over an isothermal stretching sheet with suction or injection

Aminreza Noghrehabadi [a,*], Mohammad Ghalambaz [a], Mehdi Ghalambaz[b] and Afshin Ghanbarzadeh[a]

[a]*Department of Mechanical Engineering, Shahid Chamran University of Ahvaz, Ahvaz, Iran.*
[b]*Engineering Section of Iman Madar Naslaha Co. (IMEN), Ahvaz, Iran.*

Article info:
Received: 03/02/2012
Accepted: 15/07/2012
Online: 11/09/2012

Keywords:
Nanofluids,
Stretching sheet,
Thermal enhancement,
Wall mass transfer,
Analytical solution

Abstract

In the present paper, the flow and heat transfer of two types of nanofluids, namely, silver-water and silicon dioxide-water, were theoretically analyzed over an isothermal continues stretching sheet. To this purpose, the governing partial differential equations were converted to a set of nonlinear differential equations using similarity transforms and were then analytically solved. It was found that the magnitude of velocity profiles in the case of SiO_2-water nanofluid was higher than that of Ag-water nanofluid. The results showed that the increase of nanoparticle volume fraction increased the non-dimensional temperature and thickness of thermal boundary layer. In both cases of silver and silicon dioxide, increase of nanoparticle volume fraction increased the reduced Nusselt number and shear stress. It was also demonstrated that the increase of the reduced Nusselt number was higher for silicon dioxide nanoparticles than silver nanoparticles. However, the thermal conductivity of silver was much higher than that of silicon dioxide.

Nomenclature

a	Parameter of Padé method
c	Coefficient of stretching sheet velocity
C_f	Skin friction coefficient
C_p	Specific heat at constant pressure
e_1, e_2	Parameters of symbolic power series method
f	Dimensionless flow
k	Thermal conductivity
K	A constant
L	Degree of denominator in Padé method
M	Degree of numerator in Padé method
Nur	Reduced Nusselt number
p	Parameter of Padé method
Pr	Prandtl number
q	Parameter of Padé method
Re_x	Local Reynolds number
s	Mass transfer parameter
Sh_x	Local Sherwood number
T	Temperature
T_∞	Ambient temperature
T_w	Temperature at the stretching sheet
U, U_w	Local velocity of the sheet
u,v	Velocity components along x- and y-axes

[*]*Corresponding author.*
Email address: a.r.noghrehabadi@scu.ac.ir

v_w	Velocity in y direction on the sheet surface
x,y	Cartesian coordinates (x-axis is aligned along the stretching surface and y-axis is normal to it)

Greek

α	Thermal diffusivity
ζ, γ, β	Function variables
η	Similarity variable
θ	Dimensionless temperature
λ	Avariable which shows the effect of nano particles in the momentum equation
μ	Dynamic viscosity
ρ	Density
τ	A variable defined by Eq. (25)
υ	Kinematics viscosity
φ	Nanoparticle volume fraction

Subscripts

∞	Ambient value
f	Pure fluid property
l, k	Parameters of Padé method
n	Value at the previous step
nf	Nanofluid property
s	Solid nanoparticle property
w	The stretching sheet (wall)

1. Introduction

The flow and heat transfer of a viscous fluid over a continues stretching surface have promising applications in a number of technological processes such as metal and polymer extrusion, continuous casting, drawing of plastic sheets, paper production, etc. [1 and 2]. In these applications, the heat transfer rate in the boundary layer over stretching sheet is important because the quality of the final product depends on the heat transfer rate between the stretching surface and the fluid during the cooling or heating process [3]. Therefore, the choice of a proper cooling/heating liquid is essential as it has a direct impact on the rate of heat transfer.

Recently, convective heat transfer in nanofuids has become a topic of major contemporary interest because of the unique thermal properties of these fluids. Nanofuids can be described as a fluid in which the particles in the size of nanometer, 1–100 nm, are suspended. Nanofluids were first coined by Choi [4] in 1995. Dispersed uniformly and suspended stably in a pure base fluid, a very small amount of nanoparticles can provide impressive improvement in the thermal properties of the base fluid [5].

Based on the application of nanofluids, nanoparticles have been made of various materials such as oxide ceramics, nitride ceramics, carbide ceramics, metals, semiconductors, carbon nanotubes as well as composite materials such as alloyed nanoparticles $Al_{70}Cu_{30}$ or nanoparticle core–polymer shell composites, etc. [5].

The boundary layer flow and heat transfer past a stretching sheet have received a wide range of attention among researchers. Crane [6] was the first who obtained an analytical solution for laminar boundary layer flow past a stretching sheet. Gupta and Gupta [7] solved the boundary layer flow over a stretching sheet with suction and injection. After these pioneering works, a large number of studies have been developed to analyze various aspects of this phenomenon such as magnetic flows [8], micropolar fluids [9] and viscoelastic flows [10 and 11].

Khan and Pop [12] examined boundary layer and heat transfer of nanofluids over a linear stretching sheet. Makinde and Aziz [13] analyzed heat transfer of nanofluids over a stretching sheet subjected to convective heat transfer. Rana and Bhargava [14] studied the boundary layer and heat transfer of nanofluids over a nonlinear stretching sheet.

Noghrehabadi et al. [15] investigated the thermal enhancement of nanofluids over an isothermal stretching sheet. They considered a slip boundary condition for the flow over the stretching sheet in the presence of nanoparticles. All of these studies [12–15] analyzed the effect of parametric variation of non-dimensional parameters on the thermal enhancement of nanofluids. They did not perform any case study to show the enhancement of using nanofluids in comparison with pure base fluid. In contrast, some researchers have performed case studies to indicate the enhancement of using nanofluids in comparison with the pure base fluid. Yacob et al. [16] used a numerical analysis to compare the thermal enhancement of two types of nanofluids, namely, Ag-water and Cu-water nanofluids, over

an impermeable stretching sheet. Hamad [17] studied boundary layer and heat transfer of nanofluids over an impermeable isothermal stretching sheet for the metallic and metallic oxide nanoparticles.

The purpose of the present study is to analyze the effect of two types of nanoparticles, namely, silicon dioxide and silver, on the thermal enhancement of water base nanofluids over an isothermal stretching sheet with suction or blowing. A similarity solution, depending on the volume fraction of nanoparticles, is obtained and analytically solved.

2. Problem Formulation

Consider an incompressible laminar steady two-dimensional boundary layer flow past an isothermal stretching sheet in a water-based nanofluid. The nanofluid can contain different volume fractions of SiO_2 or Ag nanoparticles. The scheme of the physical model and geometrical coordinates are shown in Fig. 1. It is assumed that the base fluid (i.e. water) and the nanoparticles are in thermal equilibrium, and also no slip occurs between them. The thermophysical properties of the water and nanoparticles are given in Table 1.

Table 1. Thermophysical properties of water and nanoparticles.

Physical Properties	Fluid Phase (water) [15]	Ag [18]	SiO_2 [19]
C_p (J/kg.K)	4179	235	765
ρ (kg/m^3)	997.1	10500	3970
k (W/m.K)	0.613	429	36
α ×10^7 (m^2/s)	1.47	1738.6	118.536

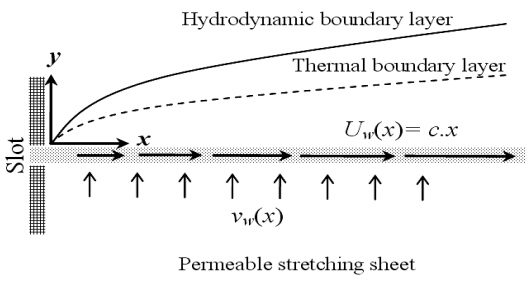

Fig. 1. Scheme of stretching sheet.

The sheet surface has the constant temperature of T_w, and the temperature of ambient fluid is T_∞. The fluid outside the boundary layer is quiescent and the stretching sheet velocity is linear. Therefore, the velocity of the sheet is $U(x)=c.x$, where c is a constant. By applying boundary layer assumptions, the steady two-dimensional boundary layer equations of the momentum, flow and heat for the nanofluid in the Cartesian coordinate system are written as:

$$\frac{\partial u}{\partial x}+\frac{\partial v}{\partial y}=0 \tag{1}$$

$$u\frac{\partial u}{\partial x}+v\frac{\partial u}{\partial y}=\frac{\mu_{nf}}{\rho_{nf}}\left(\frac{\partial^2 u}{\partial y^2}\right) \tag{2}$$

$$u\frac{\partial T}{\partial x}+v\frac{\partial T}{\partial y}=\alpha_{nf}\frac{\partial^2 T}{\partial y^2} \tag{3}$$

subject to the following boundary conditions at the sheet surface:

$$v=v_w(x),\ \ u=U_W(x),\ \ T=T_W,\ \ at\ y=0 \tag{4}$$

and the boundary conditions in the far field (i.e. y→∞):

$$v=u=0,\quad T=T_\infty\ ,\quad as\ y\to\infty \tag{5}$$

where the subscript of *nf* denotes nanofluid. The thermophysical properties of nanofluid can be evaluated as follows:

$$\alpha_{nf}=k_{nf}\big/\left(\rho C_P\right)_{nf}\ , \tag{6}$$

$$\rho_{nf}=\left(1-\phi\right)\rho_f+\phi\rho_s\ , \tag{7}$$

The effective dynamic viscosity of nanofluids can be obtained using Brinkman model [20 and 21] as:

$$\mu_{nf}=\frac{\mu_f}{\left(1-\phi\right)^{\frac{5}{2}}}\ , \tag{8}$$

and $(\rho C_p)_{nf}$ [16] as:

$$\left(\rho C_p\right)_{nf} = (1-\phi)\left(\rho C_P\right)_f + \phi\left(\rho C_p\right)_s \qquad (9)$$

The nanofluid thermal conductivity can be evaluated using Maxwell model as [22]:

$$\frac{k_{nf}}{k_f} = \frac{\left(k_s + 2k_f\right) - 2\phi\left(k_f - k_s\right)}{\left(k_s + 2k_f\right) + \phi\left(k_f - k_s\right)} \qquad (10)$$

where subscripts *f* and *s* represent the base fluid and nanoparticle, respectively. Here, φ denotes the nanoparticles' volume fraction. In order to attain a similarity solution for Eqs. (1 –3) subject to Eqs. (4 and 5), the dimensionless variables can be introduced in the following form [16–18]:

$$\begin{cases} \eta = \left(\dfrac{c}{\upsilon_f}\right)^{1/2} y, \ \theta(\eta) = \dfrac{T - T_\infty}{T_W - T_\infty}, \\ u = cxf'(\eta), \ v = -\sqrt{c\upsilon_f}\, f(\eta), \end{cases} \qquad (11)$$

where the wall mass transfer velocity becomes:

$$v_w(x) = \sqrt{c\upsilon_f}\, f(0).$$

By applying the introduced similarity transforms, Eq. (11), on the governing equations, Eqs. (1–3), the similarity equations are obtained as follows:

$$\frac{(1-\phi)^{-\frac{5}{2}}}{\left(1-\phi+\phi\,\rho_s/\rho_f\right)} f''' + f\, f'' - f'^2 = 0 \qquad (12)$$

$$\frac{\dfrac{\left(k_s + 2k_f\right) - 2\phi\left(k_f - k_s\right)}{\left(k_s + 2k_f\right) + \phi\left(k_f - k_s\right)}}{Pr\left(1-\phi+\phi\dfrac{\left(\rho C_p\right)_s}{\left(\rho C_p\right)_f}\right)} \theta'' + f\,\theta' = 0, \qquad (13)$$

subject to the following boundary conditions:

$$At\ \eta = 0\ :\ f = s, \qquad f' = 1, \qquad \theta = 1, \qquad (14)$$

$$At\ \eta \to \infty\ :\ f' = 0, \qquad \theta = 0, \qquad (15)$$

where $s = -v_w(x)\big/\sqrt{c\upsilon_f}$. The positive value of *s* indicates wall mass suction and its negative value indicates wall mass injection.

For practical purposes, the skin friction coefficient can be introduced as:

$$\begin{aligned} C_f &= -\frac{\mu_{nf}}{\rho_f U_w^2}\left(\frac{\partial u}{\partial y}\right)_{y=0}, \\ C_f &= \frac{1}{(1-\phi)^{\frac{5}{2}}}\sqrt{\mathrm{Re}_x}\, f''(0), \end{aligned} \qquad (16\text{–a})$$

where,

$$\frac{C_f}{\sqrt{\mathrm{Re}_x}} = \frac{f''(0)}{(1-\phi)^{\frac{5}{2}}}, \qquad (16\text{–b})$$

and the reduced Nusselt number as [16–18]:

$$\begin{aligned} Nu_x &= -k_{nf}\frac{x}{k_f\left(T_w - T_\infty\right)}\left(\frac{\partial T}{\partial y}\right)_{y=0}, \\ Nu_x &= -\sqrt{\mathrm{Re}_x}\,\frac{k_{nf}}{k_f}\theta'(0), \end{aligned} \qquad (17\text{–a})$$

where:

$$Nur = \frac{Nu_x}{\sqrt{\mathrm{Re}_x}} = -\frac{k_{nf}}{k_f}\theta'(0) \qquad (17\text{–b})$$

3. Solution

3.1 The Flow Analysis

Here, in order to obtain an exact close form solution for the momentum equation, Eq. (12) is rewritten in the following form for convenience:

$$\lambda f''' + f\, f'' - f'^2 = 0 \qquad (18\text{–a})$$

where:

$$\lambda = \frac{1}{(1-\phi)^{\frac{5}{2}}\left(1-\phi+\phi\,\rho_s/\rho_f\right)} \qquad (18\text{–b})$$

Assuming that the solution of (18–a) has the following form:

$$f(\eta) = \zeta + \gamma e^{-\beta\eta} \qquad (19)$$

By substituting (14) in (19), the following relations are obtained:

$$\gamma = -\frac{1}{\beta} \qquad (20\text{–a})$$

$$\zeta = s + \frac{1}{\beta} \qquad (20\text{–b})$$

Equation (15) also only holds true for positive values of β. Substituting Eq. (19) in Eq. (18–a) results in:

$$e^{-\beta\eta}\left(\lambda\beta^2 - s\beta - 1\right) = 0 \qquad (20\text{–c})$$

Solving for β leads to:

$$\beta = \frac{s \pm \sqrt{s^2+4\lambda}}{2\lambda} \qquad (20\text{–d})$$

As only the positive values of β are acceptable, the exact close form solution of Eq. (12) can be summarized as follows:

$$f(\eta) = s + \frac{2\lambda}{s+\sqrt{s^2+4\lambda}} - \frac{2\lambda e^{-\frac{s+\sqrt{s^2+4\lambda}}{2\lambda}\eta}}{s+\sqrt{s^2+4\lambda}} \qquad (21)$$

3.2 The Heat Transfer Analysis

Equation (13) subject to Eqs. (14 and 15) can be solved using a symbolic power series enhanced by Padé approximation. The basic idea of symbolic power series method and Padé approximation was explained in [23–29]. Now, the second-order differential equation of Eq. (13) can be written as two first-order differential equations:

$$\begin{aligned} &\theta_1'(\eta) - \theta_2(\eta) = 0, \\ &\theta_2'(\eta) + \frac{f\,\theta_2(\eta)}{\tau} = 0, \end{aligned} \qquad (22)$$

subject to the following boundary conditions:

$$\theta(0) = 1, \qquad \theta'(0) = K, \qquad (23)$$

under the following constraint:

$$\theta_2(\infty) = 0, \qquad (24)$$

where:

$$\tau = \left[\frac{1}{Pr}\frac{\left(k_s+2k_f\right)-2\phi\left(k_f-k_s\right)}{\left(k_s+2k_f\right)+\phi\left(k_f-k_s\right)}\right] \times \left[\frac{1}{\left(1-\phi+\phi\left(\rho C_p\right)_s/\left(\rho C_p\right)_f\right)}\right] \qquad (25)$$

Here, K is a constant which will be later computed from the boundary condition Eq. (24). In the previous section, an exact close form solution was obtained for the flow, i.e. Eq. (21), which could be substituted in Eq. (22). Therefore, Eq. (22) is only a function of θ and η. Now, the set of first-order differential equations must be solved. Based on the method of symbolic power series introduced by Celik and Bayram [29], the solution procedure is started as follows:

$$\begin{aligned} &\theta_1(\eta) = 1 + e_1\eta, \\ &\theta_2(\eta) = K + e_2\eta\ , \end{aligned} \qquad (26)$$

Substituting Eq. (26) in Eq. (22) and neglecting higher order terms yields:

$$\begin{aligned} &e_1 - K - e_2\eta = 0, \\ &e_2 - \frac{K.s}{\tau} = 0, \end{aligned} \qquad (27)$$

Solving Eq. (27) for e_1 and e_2:

$$e_1 = K,$$
$$e_2 = \frac{K.s}{\tau}, \tag{28}$$

Now, substituting e_1 and e_2 in Eq. (26) and considering a higher order term yields:

$$\theta_1(\eta) = 1 + K.\eta + e_1\eta^2,$$
$$\theta_2(\eta) = K + \frac{K.s}{\tau}\eta + e_2\eta^2 \ , \tag{29}$$

Again, substituting Eq. (29) in Eq. (22) and neglecting higher order terms yields:

$$2e_1 - \frac{K.s}{\tau} = 0,$$
$$2e_2 - \frac{k + \frac{K.s^2}{\tau}}{\tau} = 0 \ , \tag{30}$$

Solving for e_1 and e_2:

$$e_1 = \frac{K.s}{2\tau},$$
$$e_2 = \frac{K.s^2 + \tau.K}{2\tau^2}, \tag{31}$$

By substituting e_1 and e_2 in Eq. (29), considering higher terms and repeating this procedure, the following power series for θ_1 is obtained after six iterations:

$$\theta_1(\eta) = 1 + K\eta + \frac{Ks}{2\tau}\eta^2 + \frac{Ks^2 + K\tau}{6\tau^2}\eta^3$$
$$- \left(\frac{K\tau^2\left(s^2 + 4\lambda\right)^{\frac{1}{2}} - 2K\lambda s^3 + K\tau^2 s - 6K\lambda\tau s}{48\lambda\tau^3} \right)\eta^4$$
$$+ \frac{\left(\begin{array}{l} 2K\lambda^2 s^4 + K\tau^3 s^2 + 2K\lambda\tau^3 + 6K\lambda^2\tau^2 \\ -4K\lambda\tau^2 s^2 + 12K\lambda^2\tau s^2 \\ +K\tau^3 s\left(s^2 + 4\lambda\right)^{\frac{1}{2}} - 4K\lambda\tau^2 s\left(s^2 + 4\lambda\right)^{\frac{1}{2}} \end{array} \right)}{\left(240\lambda^2\tau^4\right)}\eta^5$$
$$+ O(\eta^6) \tag{32}$$

Continuing this procedure led to a symbolic power series with higher terms, in which the variable of K was unknown. In order to evaluate the value of K, the remaining unused boundary condition, i.e. Eq. (24), was used. The symbolic calculations were carried out using Maple mathematical software for convenience. For instance, by solving Eq. (22) with the boundary conditions of Eq. (23) and then applying the remaining boundary condition, Eq. (24), the following power series solution was obtained for silicon dioxide and s=1, Pr=6.2, φ =0.2:

$$\theta(\eta) = 1\text{-}4.027439000\eta$$
$$+6.928558725\eta^2\text{-}5.636791717\eta^3$$
$$\text{-}0.00009090303927\eta^4 + 4.982198443\eta^5$$
$$\text{-}5.003620742\eta^6 + 1.129018507\eta^7$$
$$+2.328223322\eta^8\text{-}2.768260327\eta^9$$
$$+1.039149690\eta^{10} + 0.6319634838\eta^{11}$$
$$\text{-}1.059090450\eta^{12} + 0.5546818207\eta^{13}$$
$$+0.04759723421\eta^{14}\text{-}0.2850366517\eta^{15}$$
$$+0.2033289427\eta^{16}\text{-}0.04054615577\eta^{17}$$
$$\text{-}0.04962873621\eta^{18} + 0.05347557267\eta^{19}$$
$$\text{-}0.02199874681\eta^{20} + O\left(\eta^{21}\right) \tag{33}$$

The obtained power series (i.e. Eq. (33)) has a sufficient accuracy, but series solutions usually have a finite range of convergence. Hence, they are not always practical for large values ofη, say $\eta\to\infty$. The combination of any series solutions with the Padé approximation provides a powerful tool for handling initial or boundary value problems on infinite or semi-infinite domains [28]. In order to increase the accuracy of solution, the power series in the symbolic form and before computation of the unknown value of K, can be converted to Padé approximation.

Padé series is defined in the following form:

$$a_0 + a_1\eta + a_2\eta^2 + \cdots = \frac{p_0 + p_1\eta + p_2\eta^2 + \cdots + p_M\eta^M}{1 + q_1\eta + q_2\eta^2 + \cdots + q_L\eta^L} \tag{34}$$

Both sides of Eq. (34) are multiplied by the denominator of right-hand side of Eq. (34):

$$\begin{aligned} & a_0 + (a_1 + a_0 q_1)\eta + (a_2 + a_1 q_1 + a_0 q_2)\eta^2 \\ & \quad + \left(a_3 + \sum_{k=1}^{3} a_{l-k} q_k\right)\eta^3 + \ldots \\ & \quad + \left(a_M + \sum_{k=1}^{M} a_{l-k} q_k\right)\eta^M + \ldots \\ & \quad + \left(a_{M+L} + \sum_{k=1}^{L} a_{l-k} q_k\right)\eta^{M+L} \\ & \quad = p_0 + p_1\eta + p_2\eta^2 + \ldots + p_M\eta^M + 0 \end{aligned} \tag{35}$$

By comparing the coefficients of both sides of (35), one can find that:

$$a_l + \sum_{k=1}^{M} a_{l-k} q_k = p_l, \quad l = 0, \cdots, M \tag{36}$$

$$a_l + \sum_{k=1}^{L} a_{l-k} q_k = 0, \quad l = M+1, \cdots, M+L \tag{37}$$

M and L are the degrees of numerator and denominator in Padé series, respectively. By solving the linear equation, Eq. (37), the q_k (k=1, …, L) is determined. After that, by substituting q_k in Eq. (36), p_l (l=0, …, M) will be determined. For instance, by following this procedure, the Padé series of Eq. (32) with the size of {1, 1} for θ_1 can be obtained as follows:
From Eq. (37) with L=1 and M=1,

$$a_2 + a_1 q_1 = 0 \tag{38}$$

Solving for q_1:

$$q_1 = -\frac{a_2}{a_1} \tag{39}$$

From Eq. (36) with M=1:

$$\begin{cases} p_0 = a_0 \\ p_1 = a_1 + a_0 q_1 \end{cases} \tag{40}$$

By substituting Eq. (39) in Eq. (40):

$$\begin{cases} p_0 = a_0 \\ p_1 = a_1 - \dfrac{a_0 a_2}{a_1} \end{cases} \tag{41}$$

By substituting Eqs. (39 and 41) in Eq. (34),

$$\frac{a_0 + a_1 - \dfrac{a_0 a_2}{a_1}\eta}{1 + -\dfrac{a_2}{a_1}\eta} \tag{42}$$

Substituting the symbolic values of a_0, a_1 and a_2 from Eq. (32) in Eq. (42) results in the Padé series of θ_1 with the size of {1, 1}:

$$\theta_1(\eta) = \frac{2\tau + (2K\tau - s)\eta}{2\tau - s\eta} \tag{43}$$

Similarly, for Padé series of θ_1 with the size of {2, 2}:
From Eq. (37) with L=2 and M=2:

$$\begin{cases} a_3 + a_2 q_1 + a_1 q_2 = 0 \\ a_4 + a_3 q_1 + a_2 q_2 = 0 \end{cases} \tag{44}$$

Solving for q_1 and q_2:

$$q_1 = \frac{a_2 a_3 - a_1 a_4}{a_1 a_3 - a_2^2}, \qquad q_2 = \frac{a_2 a_4 - a_3^2}{a_1 a_3 - a_2^2} \tag{45}$$

From Eq. (36) with M=2:

$$\begin{cases} p_0 = a_0 \\ p_1 = a_1 + a_0 q_1 \\ p_2 = a_2 + a_1 q_1 + a_0 q_2 \end{cases} \tag{46}$$

After substituting the obtained coefficients and simplification, the Padé series of θ_1 with the size of {2, 2} becomes as follows:

$$\theta_1(\eta)=$$

$$\frac{\left[\begin{array}{l}\left(2304\lambda\tau^3-1152\lambda\tau^2s^2\right)\\+\left(\begin{array}{l}2304K\lambda\tau^3-1152K\lambda\tau^2s^2\\-576\lambda\tau^2s+576\lambda\tau s^3\\+288\tau^3s+288\tau^3\sqrt{s^2+4\lambda}\end{array}\right)\eta\\+\left(\begin{array}{l}576K\lambda\tau^2s-384\lambda\tau^2+96\lambda\tau s^2\\+288K\tau^3\sqrt{s^2+4\lambda}-96\lambda s^4\\+288K\tau^3s-144\tau^2s\sqrt{s^2+4\lambda}\\-144\tau^2s^2\end{array}\right)\eta^2\end{array}\right]}{48\left[\begin{array}{l}\left(48\lambda\tau^3-24\lambda\tau^2s^2\right)\\+\left(\begin{array}{l}12\lambda\tau s^3-12\lambda\tau^2s\\+6\tau^3\sqrt{s^2+4\lambda}+6\tau^3s\end{array}\right)\eta\\+\left(\begin{array}{l}2\lambda\tau s^2-8\lambda\tau^2-2\lambda s^4\\-3\tau^2s\sqrt{s^2+4\lambda}-3\tau^2s^2\end{array}\right)\eta^2\end{array}\right]} \quad (47)$$

If the order of Padé approximation increases, the accuracy of the solution increases [26 and 27]. A comparison between power series solution, Padé approximation and numerical solution is shown in Fig. 2 for silicon dioxide and s=1, Pr=6.2, φ =0.2. The numerical solution is obtained from the solution of Eq. (13) subject to the boundary conditions Eqs. (14 and 15) using the Runge-Kutta method with shooting technique [30].

In the numerical method, the asymptotic value of η is taken as 10 to simulate the asymptotically far filed boundary condition. Figure 2 demonstrates that the Padé approximation for s=1 and φ =0.2 with the size of {8, 8} has sufficient accuracy. Hence, the {8, 8} Padé approximation is used in the following calculations. The corresponding Padé approximation of Eq. (33) can be summarized as:

$$\theta_1(\eta)=$$

$$\frac{\left(\begin{array}{l}1\text{-}1.389177547\eta+0.3621114887\eta^2\\+0.3784170075\eta^3\text{-}0.1654205827\eta^4\\-0.1657939679\eta^5+0.1753260993\eta^6\\-0.06547256744\eta^7+0.009623072673\eta^8\end{array}\right)}{\left(\begin{array}{l}1+2.638261453\eta+4.058989831\eta^2\\+4.083193261\eta^3+3.027863003\eta^4\\+1.635816922\eta^5+.6605099075\eta^6\\+0.1777898643\eta^7+0.02981101344\eta^8\end{array}\right)}, \quad (48)$$

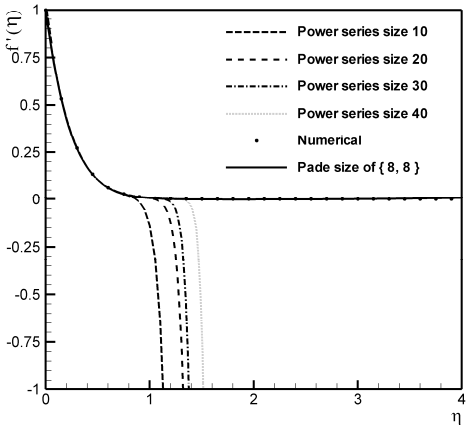

Fig. 2. Comparison of numerical, power series and Padé methods.

4. **Results and discussion**

The flow and heat equations were solved for variation of volume fraction of SiO_2 and Ag nanoparticles. In the following calculations, the Prandtl number of the base fluid (water) was kept constant at 6.2. It is worth mentioning that, when φ = 0 and s=0, this study was reduced to that of a regular viscous fluid over an isothermal impermeable stretching sheet. As a test of the accuracy of the solution, the analytical results of the present method were compared with the results reported by Hamad [17] and Wang [31] as well as those of Gorla and Sidawi [32] in the case of pure fluid, as shown in Table 2.

Furthermore, the analytical results of the present work were compared with the results reported by Hamad [17] in the case of s=0 and Ag-water nanofluid, as given in Table 3. Tables 2 and 3 indicate good agreement between the present results and the previous ones. Table 4 shows the variation of $-f''(0)$ and $-\theta'(0)$, flow and heat transfer characteristics, for different values of nanoparticle volume fractions and wall mass transfer parameter. The results of this table reveal that the increase of mass transfer parameter increases the magnitude of $-f''(0)$ and $-\theta'(0)$. Furthermore, increase of nanoparticle volume fraction increases the magnitude of $-f''(0)$ but decreases the magnitude of $-\theta'(0)$.

The non-dimensional velocity profiles for different values of silver and silicon dioxide nanoparticle volume fractions are plotted in Figs. 3 and 4, respectively. These figures interestingly show that the increase of nanoparticle volume fraction decreases the dimensionless velocity magnitude in the case of Ag-water nanofluid; however, it increases the dimensionless velocity magnitude in the case SiO_2- water nanofluid. This difference between the behavior of Ag-water and SiO_2-water nanofluids is because of the difference between density ratios of the proposed nanoparticles to the density of water, which affects the momentum equation.

In both cases of silver and silicon dioxide nanofluids, increase of mass transfer parameter (from injection to suction) decreased the magnitude of velocity profiles and hydrodynamic boundary layer. In both cases of Ag-water and SiO_2-water nanofluids, variation of nanoparticle volume fraction had no significant effect on the thickness of hydrodynamic boundary layer over the stretching sheet. Comparison between Figs. 3 and 4 shows that the magnitude of velocity profiles in the case of SiO_2 water base nanofluid was higher than that of Ag-water nanofluid.

Table 2. Comparison of the results for $-\theta'(0)$ with previous works.

Pr	Hamad [17]	Wang [31]	Gorla et al. [32]	Present Results φ=0
2	0.91136	0.9114	0.9114	0.9131
7	1.89540	1.8954	1.8905	1.9051
20	3.35390	3.3539	3.3539	3.3551
70	6.46220	6.4622	6.4622	6.4640

Table 3. Comparison of the results for $-f''(0)$ and $-\theta'(0)$ with previous works for the selected nanoparticle volume fraction of Ag nanoparticles when Pr = 6.2 and s=0.

φ	$-f''(0)$		$-\theta'(0)$	
	Hamad [17]	Present work	Hamad [17]	Present work
0.05	1.13966	1.139659	1.58136	1.581450
0.1	1.22507	1.225068	1.42058	1.420600
0.15	1.27215	1.272152	1.28193	1.282005
0.2	1.28979	1.289787	1.16100	1.161341

Table 4. Comparison between the evaluated results of $-f''(0)$ and $-\theta'(0)$ for SiO_2 and Ag nanoparticles for different values of nanoparticle volume fraction and wall mass transfer parameter.

φ	**$-f''(0)$**			
	s= – 0.5	**s= 0.5**	**s= 3**	**s= 10**
0	0.78078	1.28078	3.30278	10.09902
0.05	0.86031	1.50972	4.20532	13.08748
0.1	0.90604	1.65643	4.81412	15.10726
0.15	0.93035	1.73953	5.16826	16.28312
0.2	0.93929	1.77107	5.30428	16.73494

φ	**$-\theta'(0)$**			
	s= – 0.5	**s= 0.5**	**s= 3**	**s= 10**
0	0.33415	4.13375	18.87699	62.08581
0.05	0.33750	3.56861	16.00329	52.56564
0.1	0.34125	3.09902	13.63716	44.73115
0.15	0.34415	2.70365	11.66238	38.19476
0.2	0.34582	2.36732	9.99572	32.67934

The non-dimensional temperature profiles for the selected values of nanoparticle volume fractions are given in Figs. 5 and 6 for Ag- and SiO_2- water base nanofluids, respectively. These figures show that increase of nanoparticle volume fraction increased the non-dimensional

temperature and thermal boundary layer thickness. The addition of nanoparticles volume fraction increased the thermal conductivity of the pure fluid; hence, it resulted in the increase of thermal diffusion in the boundary layer in both types of the investigated nanoparticles. However, it had opposing differences on the velocity profiles. Increase of wall mass parameter decreased θ profiles as well as thermal boundary layer thickness.

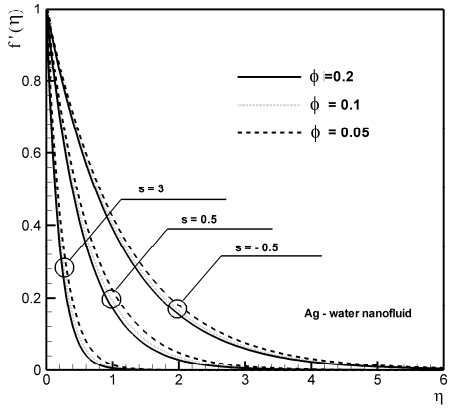

Fig. 3. Profiles of non-dimensional velocity for the selected values of volume fraction of Ag nanoparticles and mass transfer parameter.

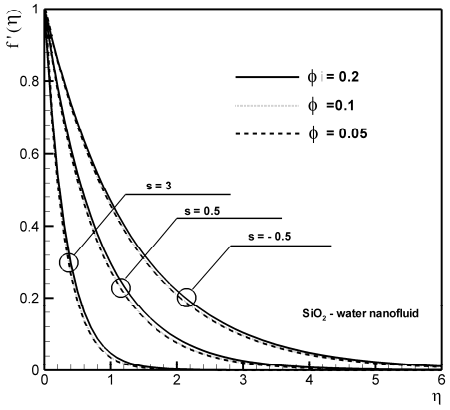

Fig. 4. Profiles of non-dimensional velocity for the selected values of volume fraction of SiO_2 nanoparticles and mass transfer parameter.

Comparison between Figs. 5 and 6 shows that the non-dimensional temperature profiles in the case of silver nanoparticles were higher than those of silicon dioxide. The variation of local skin friction and reduced Nusselt number, as important parameters of hydrodynamic and thermal boundary layer, against the variation of nanoparticle volume fraction are shown in Figs. 7 and 8 for the selected values of wall mass transfer.

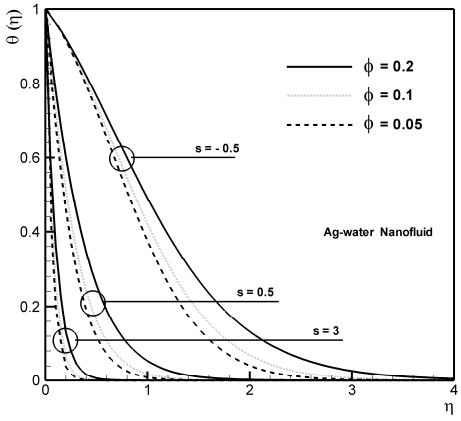

Fig. 5. Profiles of dimensionless temperature for the selected values of volume fraction of Ag nanoparticles and mass transfer parameter.

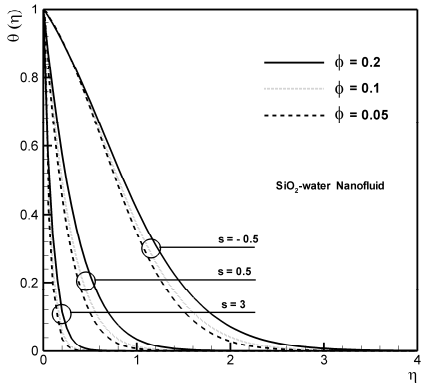

Fig. 6. Profiles of dimensionless temperature for the selected values of volume fraction of SiO_2 nanoparticles and mass transfer parameter.

Figure 7 shows that the local skin friction of Ag-water nanofluid is always higher than that of SiO_2 for the same magnitude of nanoparticle volume fraction. Increase of nanoparticle volume fraction significantly increased the local skin friction on the surface. The main part of the observed difference between these two types of

nanofluids is because of the difference between the densities of these nanoparticles (See Eq. (12)). The density of the silver nanoparticles was significantly higher than the density of silicon dioxide nanoparticles. Therefore, the presence of heavy nanoparticles resulted in the increase of local skin friction, as observed in Fig. 7. In addition, increase of wall mass transfer increased the local skin friction for two types of nanoparticles. Figure 8 demonstrates that the reduced Nusselt number for SiO_2 was higher than that for Ag for the same value of nanoparticle volume fraction.

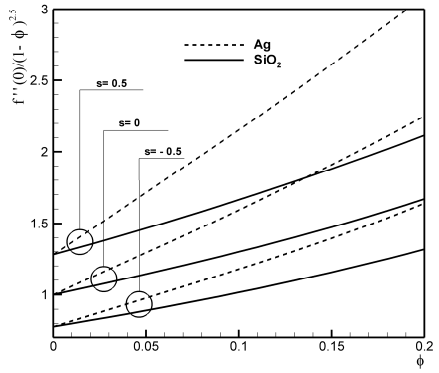

Fig. 7. Comparing the variation of local surface skin friction with variation of nanoparticle volume fraction for the selected values of wall mass transfer.

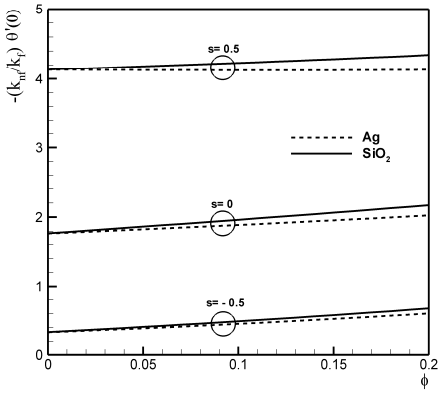

Fig. 8. Comparing the variation of reduced Nusselt number with variation of nanoparticle volume fraction for the selected values of wall mass transfer.

The increase of nanoparticle volume fraction increased the reduced Nusselt number. Increase of wall mass transfer parameter increased the difference between temperature profiles of Ag and SiO_2 nanofluids. Finally, increase of the wall mass transfer increased the reduced Nusselt number.

5. Conclusions

The effect of the presence of silver and silicon dioxide nanoparticles on the hydrodynamic and thermal boundary layer over a permeable isothermal stretching sheet was analytically investigated. A close form exact solution was obtained for the momentum equation. The heat equation was also solved using the combination of a symbolic power series and Padé approximation method. In the nanofluid model, the effect of presence of nanoparticles on the thermal conductivity and dynamic viscosity was considered. The obtained results can be summarized as follows:

The silver nanoparticles and silicon dioxide nanoparticles decreased and increased the dimensionless velocity magnitude, respectively. However, they had no significant effect on the thickness of hydrodynamic boundary layer.

The non-dimensional temperature profiles in the case of silver nanoparticles were higher than those of silicon dioxide.

Increase of nanoparticle volume fraction significantly increased the local skin friction on the sheet surface. The local skin friction of Ag-water nanofluid was always higher than that of SiO_2.

Increase of nanoparticle volume fraction increased the reduced Nusselt number. However, the reduced Nusselt number for silicon dioxide nanoparticles was higher than that of silver nanoparticles.

Finally, increase of the wall mass transfer (from injection to suction) increased the reduced Nusselt number.

Acknowledgements

The authors appreciate Shahid Chamran University of Ahvaz for its support from this paper.

References

[1] T. Altan, S. Oh and H. Gegel, *Metal forming fundamentals and applications*, American Society of Metals, Metals Park, OH, (1979).

[2] E. G. Fisher, *Extrusion of Plastics*, Wiley, New York, (1976).

[3] M. V. Karwe and Y. Jaluria, "Numerical simulation of thermal transport associated with a continuous moving flat sheet in materials processing", *ASME J. Heat Transfer*, Vol. 119, pp. 612–619, (1991).

[4] S. U. S. Choi, "Enhancing thermal conductivity of fluids with nanoparticles", *Developments and Applications of Non-Newtonian Flows*, Vol. 231, pp. 99–105, (1995).

[5] L. Godson, B. Raja, D. Mohan Lal and S. Wongwises, "Enhancement of heat transfer using nanofluids–An overview", *Renewable and Sustainable Energy Reviews*, Vol. 14, pp. 629–641, (2010).

[6] L. Crane, "Flow past a stretching plate", *Z Angew Math Phys*, Vol. 21, pp. 645–651, (1970).

[7] P. S. Gupta and A. S. Gupta, "Heat and Mass transfer on a stretching sheet with suction or blowing", *Can J Chem Eng*, Vol. 55, pp. 744–749, (1977).

[8] F. Ali, R. Nazar, N. Arifin, and I. Pop, "MHD boundary layer flow and heat transfer over a stretching sheet with induced magnetic field", *Heat and Mass Transfer*, Vol. 47, pp. 155–162, (2011).

[9] M. Ashraf and M. M. Ashraf, "MHD stagnation point flow of a micropolar fluid towards a heated surface", *Applied Mathematics and Mechanics*, Vol. 32, pp. 45–54, (2011).

[10] C. Arnold, A. Asir, S. Somasundaram, and T. Christopher, "Heat transfer in a viscoelastic boundary layer flow over a stretching sheet", *International Journal of Heat and Mass Transfer*, Vol. 53, pp. 1112–1118, (2010).

[11] M. Turkyilmazoglu, "Multiple solutions of heat and mass transfer of MHD slip flow for the viscoelastic fluid over a stretching sheet", *International Journal of Thermal Sciences*, Vol. 50, pp. 2264–2276, (2011).

[12] W. A. Khan and I. Pop, "Boundary-layer flow of a nanofluid past a stretching sheet", *International Journal of Heat and Mass Transfer*, Vol. 53, pp. 2477–2483, (2010).

[13] O. D. Makinde and A. Aziz, "Boundary layer flow of a nanofluid past a stretching sheet with a convective boundary condition", *International Journal of Thermal Sciences*, Vol. 50, pp. 1326–1332, (2011).

[14] P. Rana and R. Bhargava, "Flow and heat transfer of a nanofluid over a nonlinearly stretching sheet: A numerical study", *Communications in Nonlinear Science and Numerical Simulation*, Vol. 17, pp. 212–226, (2012).

[15] A. Noghrehabadi, R. Pourrajab and M. Ghalambaz, "Effect of partial slip boundary condition on the flow and heat transfer of nanofluids past stretching sheet prescribed constant wall temperature", *International Journal of Thermal Sciences*, Vol. 54, pp. 253–261, (2012).

[16] N. A. Yacob, A. Ishak, I. Pop and K. Vajravelu, "Boundary layer flow past a stretching/shrinking surface beneath an external uniform shear flow with a convective surface boundary condition in a nanofluid", *Nanoscale research letters*, Vol. 6, pp. 314–321, (2011).

[17] M. A. A. Hamad, "Analytical solution of natural convection flow of a nanofluid over a linearly stretching sheet in the presence of magnetic field", *International Communications in Heat and Mass Transfer*, Vol. 38, pp. 487–492, (2011).

[18] K. Vajravelu, K. V. Prasad, J. Lee, C. Lee, I. Pop and R. A. Van Gorder, "Convective heat transfer in the flow of viscous Ag–water and Cu–water nanofluids over a stretching surface", *International Journal of Thermal Sciences*, Vol. 50, pp. 843–851, (2011).

[19] G. R. Kefayati, S. F. Hosseinizadeh, M. Gorji and H. Sajjadi, "Lattice Boltzmann simulation of natural convection in tall enclosures using water/SiO2 nanofluid", *International Communications in Heat and Mass Transfer*, Vol. 38, pp. 798–805, (2011).

[20] H. C. Brinkman, "The viscosity of concentrated suspensions and solutions", *J. Chem. Phys.*, Vol. 20, pp. 571–581, (1952).

[21] K. Khanafer, and K. Vafai, "Critical synthesis of thermophysical characteristics of nanofluids", *International Journal of Heat and Mass Transfer*, Vol. 54, pp. 4410–4428, (2011).

[22] J. C. A. Maxwell, *Treatise on Electricity and Magnetism*, 2nd ed., Clarendon Press, Oxford, (1881).

[23] H. Chu, Y. Zhao and Y. Liu, "A MAPLE package of new ADM-Padé approximate solution for nonlinear problems", *Applied Mathematics and Computation*, Vol. 217, pp. 7074–7091, (2010).

[24] E. Celik and M. Bayram, "Arbitrary order numerical method for solving differential-algebraic equation by Padé series", *J. Applied Mathematics and Computation*, Vol. 137, pp. 57–65, (2003).

[25] E. Celik and M. Bayram, "The numerical solution of physical problems modeled as a systems of differential-algebraic equations (DAEs)", *J. of the Franklin Institute*, Vol. 342, pp. 1–6, (2005).

[26] N. Guzel and M. Bayram, "Numerical solution of differential–algebraic equations with index-2", *J. Applied Mathematics and Computation*, Vol. 174, pp. 1279–1289, (2006).

[27] N. Guzel and M. Bayram, "On the numerical solution of stiff systems", *Applied Mathematics and Computation*, Vol. 170, pp. 230–236, (2005).

[28] W. Wang, "An algorithm for solving DAEs with mechanization", *Applied Mathematics and Computation*, Vol. 167, pp. 1350–1372, (2005).

[29] E. Celik and M. Bayram, "On the numerical solution of diferential-algebraic equations by Padé series", *Applied Mathematics and Computation*, Vol. 137, pp. 151–160, (2003).

[30] R. L. Burden and J. D. Faires, *Numerical analysis*, 8th ed., Thomson Higher Education, Belmont, pp. 272–280, (2004).

[31] C. Y. Wang, "Free convection on a vertical stretching surface", *J. Appl. Math. Mech*, Vol. 69, pp. 418–421, (1989).

[32] R. S. R. Gorla and I. Sidawi, "Free convection on a vertical stretching surface with suction and blowing", *Appl. Sci. Res.*, Vol. 52, pp. 247–258, (1994).